HYPERCONE INFLATABLE SUPERSONIC DECELERATOR

Glen J. Brown*
Vertigo, Inc.
Lake Elsinore, California

Chirold Epp ţ, Claude Graves‡
NASA Johnson Spaceflight Center
Houston, Texas

Steve Lingard§, Matt Darley ¶
Vorticity, Ltd.
Chalgrove Oxfordshire

Keith Jordan#
Computational Fluid Dynamics Research Corp
Huntsville, Alabama

Abstract

The need for an efficient supersonic decelerator arises first for use in aero-braking planetary landers, but may also have other uses such as spacecraft crew escape and aerocapture of orbital planetary probes. Hypercone is a concept currently under investigation for use in such applications. This paper discusses the historical background of similar devices, structural concepts and requirements, aerodynamic performance up to Mach 4.0, inflation system considerations, and total mass estimates for a Mars lander case.

Background

Conventional parachutes are generally not suitable for use in supersonic conditions. The Viking parachute was tested at up to Mach 2.7, which is generally considered to be the useful upper limit for parachutes of this type. Specialized supersonic types are also known, such as Hemisflo and the general class of Ballutes, but would generally be unsuitable as large-scale decelerators because of weight.

The sphere-cone geometry typical of traditional aeroshells is known for good stability and high drag coefficient. Figure 1 compares the drag coefficient based on projected area of a number of sphere-cone examples with a disk-band-gap (DGB) parachute.

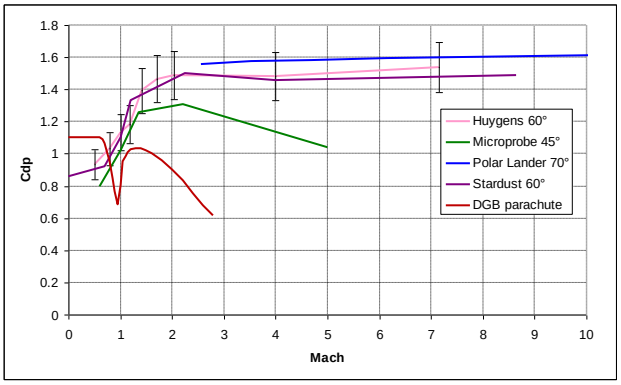

Figure 1

The idea of increasing the effective area of a sphere-cone with inflatable structures and membranes surfaces has also been put forward a number of times. Kendall has described and patented an inflatable cone for use as a recovery system that includes an inflatable hub-spoke-rim frame[1]. Another conical design, but with advances in materials and a two-stage deployment scheme, was developed by Babakin Space Center and Astrium with funding provided by ESA and is known as Inflatable Re-entry and Descent Technology (IRDT)[2]. (See Figure 2.)

---

* President, Senior Member
ţ Project Manager
‡ Principle Investigator
§ Technical Director, Senior Member
¶ Senior Engineer
# Senior Application Engineer

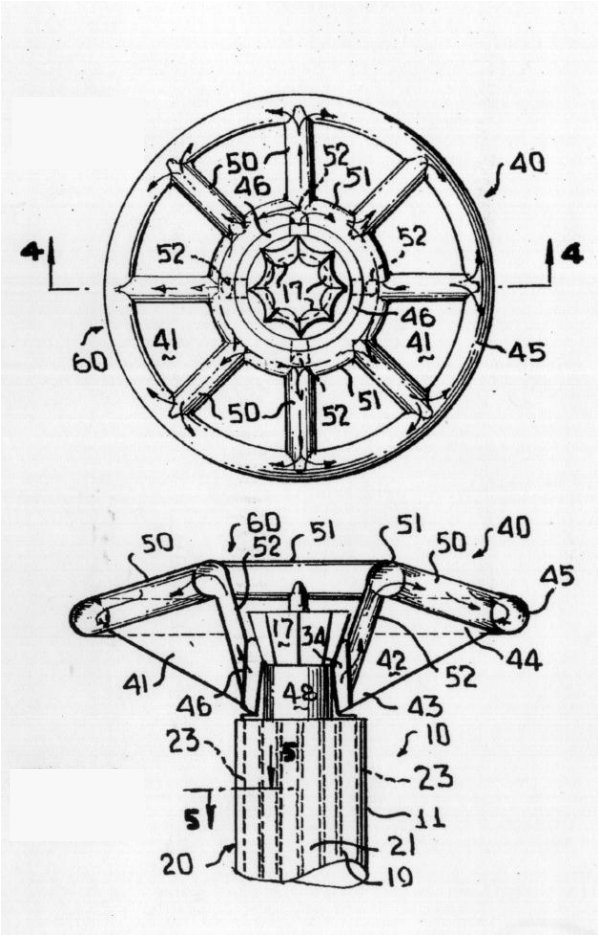

Figure 2

The common concept behind these examples of inflatable conical decelerators is the use of a conventional rigid nose cone (or forebody) in the very high temperature stagnation region, with an attached, lightweight inflatable structure deploying to increase the size and lower the ballistic coefficient of the reentry vehicle.

The Hypercone concept continues this theme, but includes advanced structural technology to greatly reduce weight and packed volume maintaining the high-drag conical surface. A single, slender inflatable torus at the rim of the cone is attached via radial tapes to the re-entry vehicle or lander. Fabric, including thermal protection material as necessary, spans the tapes to define the aerodynamic surface. (See Figure 3.)

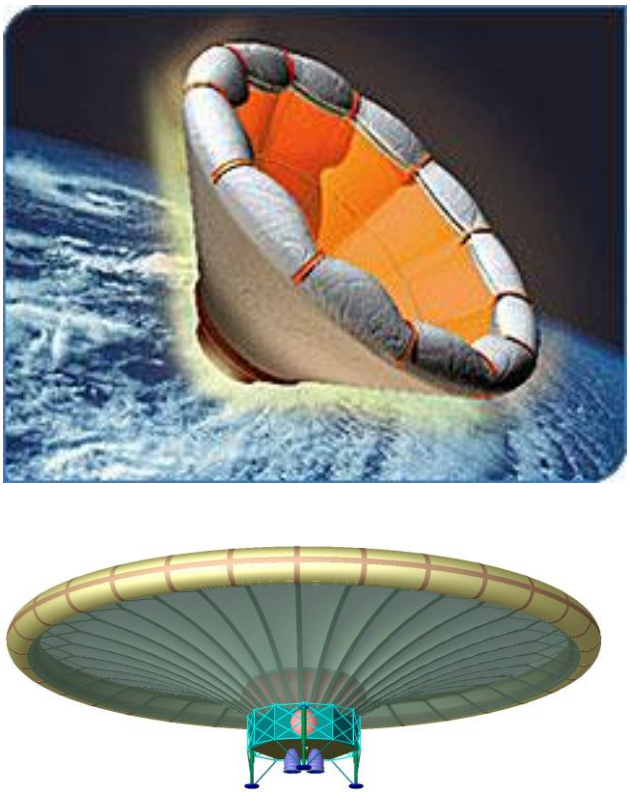

Figure 3

CFD Analysis

The model used for CFD simulation is illustrated in Figure 4. The Hypercone model represented is 14 m in diameter, has a torus with a 0.8 m diameter and a conical section with a 55° half angle. The model was constructed in LS-DYNA (commercial non-linear FEA code) with a rigid lander and torus (for speed) and a flexible cone simulated using an orthotropic fabric model. The model was loaded using a notional pressure difference across the fabric of 1600 Pa (approximately equivalent to a Mach 2.3 case). The torus was held fixed and a force 6 times the weight of the lander was uniformly applied at the interface ring to simulate deceleration of the system. Six g is the deceleration that would result from the pressure distribution. The undeformed and deformed shapes are shown in Figure 5.

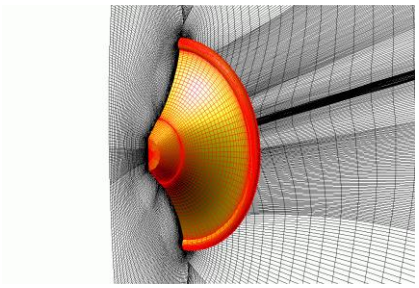

Hypercone System Surface and Symmetry Plane Meshes

Figure 4

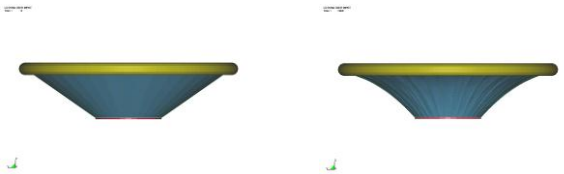

Undeformed and deformed shapes for CFD analysis

Figure 5

The density-based flow solver, CFD-FASTRAN, was used for this analysis. CFD-FASTRAN solves the full Navier-Stokes equations in a general curvilinear coordinate system employing finite-volume methods. The flow solver supports structured/unstructured, hybrid, multi-block, blocked and chimera grid systems. The solver also provides many advanced features, including modules for simulating unsteady, dynamic motion and thermo chemistry for reacting flows. Several turbulence models are supported, including the high-Reynolds number k-ε model with wall functions. Both flux-vector and flux-difference splitting schemes are employed with higher-order limiters.

This method was used to obtain the majority of the results presented here. For the particular Mars landing case being studied, the deformed shape used for the CFD was re-calculated with the derived pressure distribution at Mach 3.1 and Mach 4.0. The maximum difference in deformation between these cases and the uniform pressure distribution used for the CFD model as 1 percent or less as measured by the axial position of the torus relative to the lander.

Drag Aerodynamics

Figure 6 shows CFD drag results for the 4 MT lander and 14 m Hypercone as they vary with Mach number and angle of attack. The undeformed shape was not calculated in this study, be we have observed in earlier studies that the deformed shape has the higher drag.

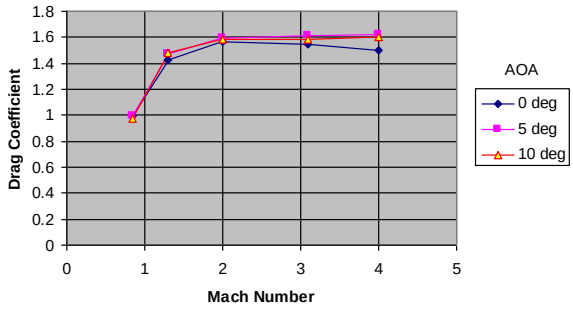

Figure 6

Aerodynamic Stability

CFD results for angles of attack up to 15 degrees were used to assess static pitch stability. The results are shown in Figure 7.

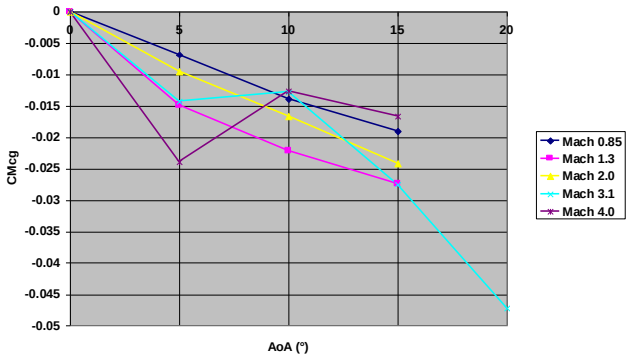

Figure 7

The configuration is stable at all Mach numbers and most of the results are consistent with engineering judgment. However, the trends of some of the pitching moment coefficients were not as expected. It was thought that a reasonably smooth trend across the Mach number range would result. However, changes in the slope of the C_m curve appear for Mach 3.1 and 4.0 (see Figure 7). Upon investigation, it was found that the changes in the slopes are caused by movement of stagnation regions at the juncture of the inflated torus and the decelerator fabric near the top, coupled with a reduction in pressure on the lower half. As the AoA exceeds 5.0 deg, a high-pressure region moves from the side toward the top of the configuration, while the pressure on the lower half of the skin drops, thus counter-acting some of the stabilizing moment. Surface pressure contour plots for M= 4.00 can be seen in Figure 8.

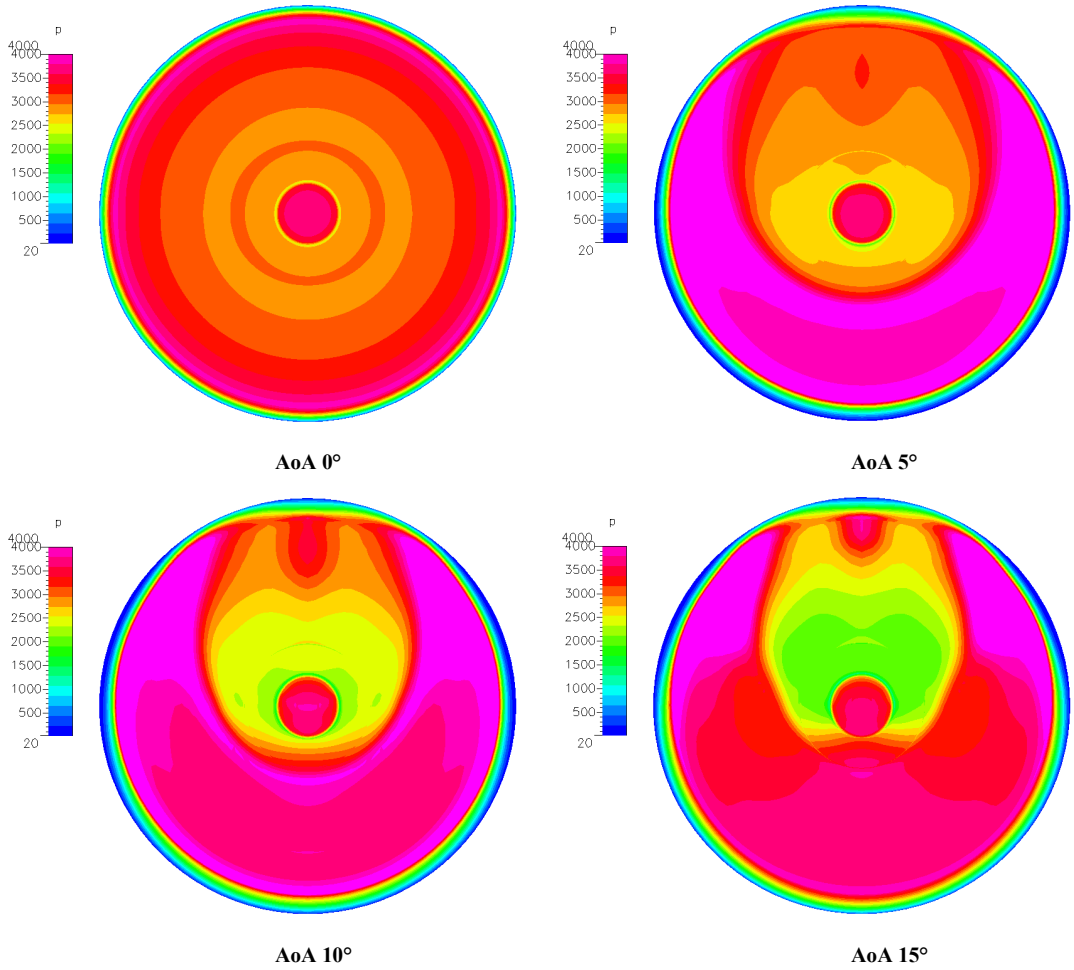

Figure 8 Front face pressure distribution at Mach 4.

We investigated the effect of the membrane-torus junction geometry on the moment curves by repeating the calculations for the three geometries illustrated in Figure 9. The conclusion was that the original geometry was actually the most stable. The smoothest geometry, in the middle position in the figure, was actually the least stable, adverse pitching moments being generated by a high total pressure stream moving around the separation bubble on the nose of the vehicle and compressing on the conical section..

Dynamic stability was evaluated, treating the Hypercone-lander as a single rigid body. Static moments from CFD and Viking pitch damping derivative (C_{Mq}) values were used[4]. Figure 10 shows the pitch motion after release at Mach 3.54 and 10 degree angle of attack in the Martian atmosphere at an altitude of 6,650 m.

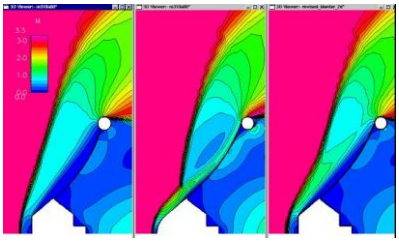

Mach plots of three Hypercone configurations at Mach 3.1 and 0°AoA

Figure 9

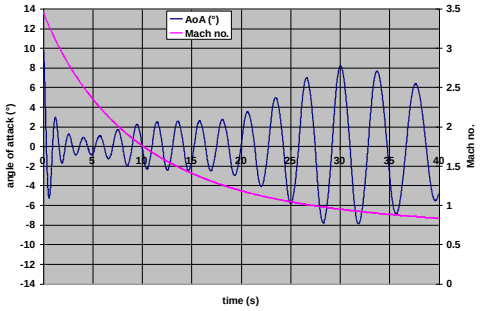

Hypercone / lander stability for deployment at Mach 3.54, 10° initial AoA

Figure 10

The results of the simulations show that the system is strongly statically stable as could be deduced from the static aerodynamic coefficients.

There is little sensitivity to realistic center of gravity movement within the lander.

Dynamic response is governed by the assumptions for C_{mq}. The values for C_{mq} were taken from the Viking data. Damping for Hypercone should be better because of the smaller cone angle and the lack of perfect coupling between the cone motion and the lander motion. Positive C_{mq} for sphere-cones in the transonic regime largely occurs because the base pressure changes lag the front face pressure changes in a coherent manner.

Structures

In part, the motivation for Hypercone stems from recent advances in manufacturing technology related to inflatable structures. Tubular geometries, seamlessly reinforced by high modulus, high tenacity fibers can be manufactured by the braiding process. The resulting bias structure has highly desirable structural characteristics when combined with non-bias (axial) reinforcements that define both the tubular shape (straight, arch, torus) and its bending stiffness. An example of such a structure is shown in Figure 11. It is a 35 m long, 0.8 m diameter tube, formed into an arch 26 m wide and 11 m tall. It is designed to support a 9,000 kg distributed load, yet weighs approximately 180 kg, uninflated. A braided, inflated torus is shown in Figure 12.

Figure 11

It is feasible to construct the type and size of seamless , reinforced torus that will be needed for Hypercone using these methods.

Figure 12

Relatively simple closed-form equations that predict bending strength and stiffness of this type of beam have been developed and validated. We have used these equations as the basis for a parametric mass model for Hypercone. The specific preliminary design was then evaluated with more sophistical, non-linear FEA tools to validate the earlier estimates.

Stability of the slender torus in compression is the key structural consideration for Hypercone. Critical bending stiffness equations for the two buckling modes have the familiar form of the Euler equation for slender columns, but with different coefficients.

•Column buckling: $C' = \frac{\pi^2 EI}{L^2}$

•Ring, in-plane buckling: $C'_{in} = \frac{12EI_{in}}{D^2}$

•Ring, out-of-plane buckling: $C'_{out} = \frac{16EI_{out}}{D^2}$

Two principle modes of buckling are identified along with their associated bending stiffness (EI) requirement for a given compressive load. The torus structure can be designed to have different bending stiffness about different transverse axes by the placement and size of the axial reinforcing fiber groups.

The ring buckling equations are modified according to interface constraints. We do not use the more accurate forms for engineering estimates because we have finite element tools that are much more accurate when the attachment loads are not smoothly distributed. This analysis has been done, however, and can be found in the references[3].

As implied by the buckling equations, the mass of material required for the torus structure is sensitive to the relationship between drag force and compression in the torus. Since this, in turn, is a strong function of cone angle. We used the parametric mass model to find the mass-optimum cone angle of the undeformed Hypercone. Figure 13 shows the variation of Hypercone mass with undeformed cone angle.

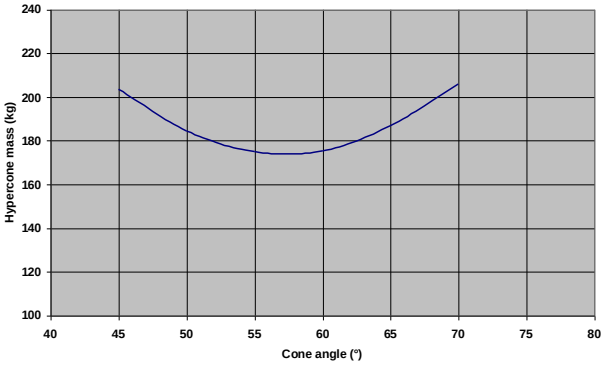

Figure 13

Based on this result, the 4 MT Mars lander study was based on a 55 degree Hypercone.

Structural Stability

As a check on our assumption that the Hypercone-lander moves as a single rigid body, a simulation was configured to apply a forced, lateral sinusoidal oscillation to the rigid torus. A uniform pressure load of 2000 Pa was applied to the cone surface and a vertical acceleration of 60 m/s2 was applied to the lander body, to generate representative loading to the Hypercone. A large degree of mass damping was applied to the structure for the first second of simulation to cause rapid convergence to the stable deformed shape. Following this, the forced oscillation was applied to the torus in the lateral x-direction, with motion of the torus constrained to this axis only. Figure 14 shows a comparison of the lateral displacement of the torus (green) and lander body (red).

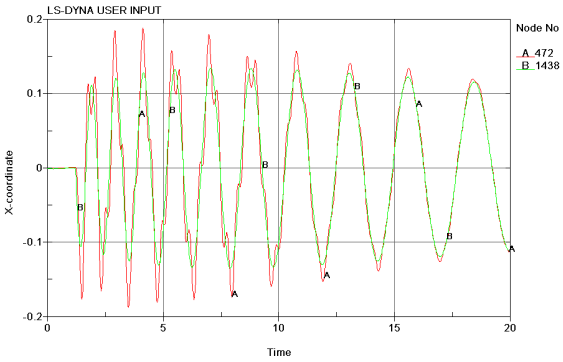

Figure 14. Coupling between lander and torus/cone during forced oscillation of the torus – displacement

The driving sinusoid was based on the predicted frequency of oscillation of the Hypercone, decreasing with time as q decreases. It can be seen that the lander motion couples strongly with torus/cone at the expected oscillation frequency range. The lander has a higher natural frequency, which is excited at the higher driving frequency towards the left of the charts, but as the oscillation frequency decreases, the lander motion couples much more closely. This method of forced oscillation is somewhat artificial as the torus was driven in the lateral plane, rather than about a rotation axis through the center of mass of the system. It was concluded however that the degree of coupling allowed the system to be sensibly considered rigid for stability analyses.

Inflation System

The inflation system components and the inflation gas constitute a significant fraction of the decelerator system mass. A quick study was conducted to review the types of inflation systems that might be considered. Some impractical types were included for comparison purposes. Table 1 summarizes the results. The mass-efficiency of a gas generator is expressed as the ratio of kg-moles of gas produced to kg of inflation system weight.

Weight and Volume Comparison of Gas Generator Types					
Type	Output	Msys/Mgas	mol. wt.	mole/kg-mole	Notes
LH2	H2	1	2.02	50%	mass lower bound, requires heating
LH2/O2 Hybrid	H2+H2O	1.1	4.56	20%	11% H2 + 89% O2 = 760 degR out
LH2/SP Hybrid	H2+CO2+H2O+…	1.25	5.84	14%	28% H2 + 72% SP = 760 degR out
Compressed gas	H2	21	2.02	2.4%	requires external heating
Solid Propellant	CO2+H2O+NOx+…	1.22	22	3.7%	requires external cooling
NH3/SP Hybrid	CO2+H2O+NH3+…	2.28	20	2.2%	50% NH3 + %50% SP = 760 degR out
Metal Hydride	H2	70	2.02	0.7%	reversible
Li+H20	H2+LiOH	42	2.02	1.2%	highly exothermic, cooling ?

Table 1

Parameters for Mass Example		
Deploy altitude	6650 m	
Deploy Mach	3.0	
Dynamic pressure	1600 Pa	(33.4 psf)
Lander mass	4843 kg	
Torus diameter	14.0 m	
Section diameter	0.8 m	
Inflation pressure	235977 Pa	(34.2 psi)

Hypercone Mass, Kg	
Gas	25.2
Inflation System	29.0
Straps	15.4
Braid	31.8
Coating	16.9
Liner	11.1
Radials	11.0
Fabric	12.0
Miscellaneous	30.5
Totals	182.9
Mass Fraction	3.8%

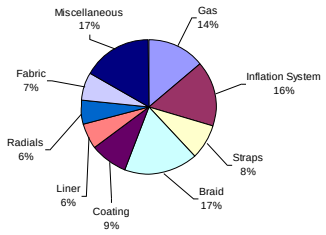

Figure 15

The lower bound is represented by LH2 vaporized to gas, with no containment, heat source or heat exchanger mass, with an efficiency of 50%. Burning some LO2 to vaporize and heat the remaining LH2, including a 10% charge for hardware, drops efficiency to 20%. Such a system might be feasible, but has no spaceflight heritage as a gas generator.

GH2 in a carbon-overwrap tank is 2.4% efficient but would discharge gas at a very low temperature. Using a solid propellant to vaporize liquid ammonia is 2.2% efficient and discharges gas at a nearly optimum, warm temperature. The solid propellant-ammonia hybrid has extensive space heritage and has been the baseline for all system mass estimates. There may well be possibilities for innovative improvements to inflation systems in the future.

Decelerator Mass

Numerous system mass estimates have been made as part of trade studies. One example is reproduced here as a representative example.

The example used is for a 4 MT Mars lander, deployed at Mach 3.0 to decelerate the lander to subsonic conditions at which point a subsonic parachute is deployed. (The two-stage system was found to be lighter then either a Hypercone alone or a hypothetical Mach 3 parachute alone.)

The weight and mass fraction shown in Figure 15 include only minimal thermal protection, that afforded by the fabric coating, because predicted peak temperature for Mars aerobraking does not require more. Other applications, such as Earth re-entry, would require additional thermal protection on the forward surface and substantial associated mass.

Conclusions

The Hypercone configuration shows promise for planetary deceleration and, perhaps, other applications. Outstanding features include high drag coefficient, aerodynamic and structural stability through at least Mach 4.0. Additional work is needed to define and show the feasibility of the needed thermal protection system for Earth atmospheric applications. Wind tunnel work is needed to validate the current findings.

References

1. Kendall at al., “Recovery System”, US Patent No. 4,832,288, May 23, 1989
2. Wilde et al., “Inflatable Reentry and Descent Technology (IRDT – Further Developments”, 2nd International Symposium of Atmospheric Reentry Vehicles and Systems, Arcachon, France, March 2001 (http://www.weblab.dlr.de/rbrt/GpsNav/IRDT/arcachon_paper.pdf)
3. Weeks, George E.,”Buckling of a Pressurized Toroidal Ring Under uniform External Loading”, NASA TN D-4124, Langley Research Center, August 1967.
4. S. Steinberg, B.L. Uselton and P.M. Siemers, ‘Viking Configuration Pitch Damping Derivatives as Influenced by Support Interference and Test Technique at Transonic and Supersonic Speeds’, AIAA 72-1012 (1972)
5. Lingard, J. S., Darley, M., Brown, G.,”Hypercone Study Final Report”, Vertigo Document 2004-11-0004, January 2003.